



UNIVERSITY OF SCIENCE AND TECHNOLOGY
OF HA NOI
MASTER SPACE AND APPLICATION
MASTER THESIS

Cosmic ray interaction with detectors of the Planck
satellite for the measurement of the cosmic microwave
background radiation polarization

Author:

Hoang Duc Thuong

Supervisor:

Asc.Prof Guillaume Patanchon

*A thesis submitted in fulfilment of the requirements
for the degree of Master Space and Application*

in the

APC-AstroParticule et Cosmologie Laboratoire
Université Paris Diderot-Paris 7

May 2017

Declaration of Authorship

I, Hoang Duc Thuong, declare that this thesis titled, '*Cosmic ray interaction with detectors of the Planck satellite for the measurement of the cosmic microwave background radiation polarization*' and the work presented in it are my own. I confirm that:

- This work was done wholly while in candidature for a research degree at APC(*AstroParticule et Cosmologie Laboratoire*)-Université Paris Diderot-Paris 7.
- Where I have consulted the published work of others, this is always clearly attributed.
- Where I have quoted from the work of others, the source is always given. With the exception of such quotations, this thesis is entirely my own work.
- I have acknowledged all main sources of help.

Signed:

Date:

Acknowledgements

I am very thankful to professor Giraud-Héraud Yannick director of APC(*AstroParticule et Cosmologie Laboratoire*) as well as Université Paris Diderot-Paris 7 and University of Science and Technology of Hanoi for giving me opportunity to work in the Paris-France.

I am also indebted to associate professor Cyrille Rosset, all members of APC and my friends through out my stay.

Above all I would like to express from my heart and gratefulness to my supervisor, associate professor Guillaume Pantachon and for his guidance and discussion during the study. He always opens the windows for me to enter.

Abstract

Cosmic ray interaction with detectors of the Planck satellite for the measurement of the cosmic microwave background radiation polarization

by HOANG DUC THUONG

The *Planck* satellite of ESA was launched 2009 from Kourou France Guyana. It measure temperature and polarization anisotropies of the cosmic microwave background radiation (CMB). Planck observes the CMB with two instruments Low Frequency Instrument and High Frequency Instrument . This work focus on the study of the cosmic rays on the Planck High Frequency Instrument. The high energy particle hitting to the silicon die of polarization sensitive bolometers (PSB) and spider wed bolometers (SWB) deposit energy and produce the *long glitches* on the scientific data. Therefore the modeling, analysis and simulation are play a vital role to understand and characterize of the long glitches. This understanding allows us to better remove the impact of the *long glitches* on polarization sensitive bolometers data.

Contents

Declaration of Authorship	i
Acknowledgements	ii
Abstract	iii
Contents	iv
List of Figures	vi
List of Tables	vii
Abbreviations	viii
1 Introduction	1
2 Cosmology, CMB and the Planck satellite	3
2.1 Cosmology and CMB	3
2.2 The Planck satellite	5
2.2.1 The HFI bolometer	9
2.2.2 Components of the HFI bolometer	10
3 Cosmic ray, interaction with detectors	12
3.1 Cosmic rays	12
3.2 Interaction of cosmic rays with the detectors	15
3.2.1 Interaction with the silicon die	16
4 Methodology	19
4.1 The simple modeling	19
4.2 Analytical approach	22
4.3 Simulation approach	25
4.4 Coincidences analysis	27
5 Result, comparison and discussion	28
5.1 Result and comparison	28

5.2 Interpretation and Discussion	31
5.3 Coincident	32
6 Conclusion	34
Bibliography	36

List of Figures

2.1	The evolution of the Universe	4
2.2	Diagram of the <i>Planck</i> satellite at the second Lagrange point	6
2.3	The main components of <i>Planck</i>	7
2.4	The footprint focal plane	7
2.5	The raw data (unprocessed)	8
2.6	<i>Top left:</i> Bolometer PSB pair (a and b)	10
2.7	A perspective drawing of a PSB, a SWB	11
3.1	Victor Hess (<i>left center</i>) and his balloon	13
3.2	The spectrum of particles per energy-per-nucleus	14
3.3	Three family of glitches for PSB on raw data	16
3.4	The CRs penetrated into Silicon die	17
3.5	Stopping power of positive muons in copper	18
3.6	The long glitches of the experiment data	18
4.1	The simple model of the coming particle	19
4.2	The PAMELA result	20
4.3	The solar sunspot in 11 years	20
4.4	The stopping power of primary cosmic rays	21
4.5	Deposit energy through n layer	22
4.6	<i>Left:</i> Flux of particle with coming energy $\frac{dN}{dE_0}$	23
4.7	The flow chart of analytical approach	24
4.8	Deposit energy of p and He between PSB pair	26
4.9	The flow chart of simulation approach	27
5.1	Spectrum of particle per deposit energy $\frac{dN}{dE}$	28
5.2	The cumulative distribution $N(> E)$ comparison	29
5.3	The long glitches of analytical (<i>left</i>) and simulation (<i>right</i>)	29
5.4	The long glitches comparison	30
5.5	The long glitches simulate in a PSB pair	31
5.6	The long glitches coincident simulate in a PSB pair	32
5.7	The long glitches coincident comparison	33

List of Tables

2.1 The HFI bolometers	9
----------------------------------	---

Abbreviations

APC	laboratoire AstroParticule et Cosmologie
CMB	Cosmic Microwave Background radiation
COBE	COsmic Background Explorer
WMAP	Wilkinson Microwave Anisotropy Probe
CRs	Cosmic Rays
HFI	High Frequency Instrument
LFI	Low Frequency Instrument
PSB	Polarization Sensitive Bolometer
SWB	Spider Web Bolometer
SREM	Standard Radiation Environment Monitor

Chapter 1

Introduction

The *Planck* satellite is a 3rd generation cosmic microwave background experiment, a mission of the European Space Agency. It was launched in May 2009 from Kourou (France Guyana) to the second Sun-Earth Lagrange point and observed the sky between August 2009 and August 2013. Planck is designed to answer key cosmological questions. It observes the tiny fluctuations of the cosmic microwave background radiation (CMB) which have average temperature 2.726K $\pm \frac{\Delta T}{T} \approx 10^{-5}$. CMB was emitted about 13 billion years ago and 370 000 years after the Big Bang. It is the oldest light in our universe. Thus CMB measurements with high angular and sensitivity play an important role to determine the evolution of structures of the universe, and the origin of primordial fluctuations, and allows to quantify dark matter and dark energy. The *Planck* satellite is composed of two instruments: The High Frequency Instrument (HFI) and the Low Frequency Instrument (LFI). The HFI instrument operates with 50 signal bolometers including twelve polarization sensitive bolometer (PSB) and unpolarization spider-web bolometers (SWB) also 16 thermometers, two dark bolometers, a resister and capacitor. Each PSB module have two bolometers back together measuring linear polarization in the range of frequency is between 100 GHz and 1 THz.

Cosmic rays (CRs) which are high energy particles interact on the 100 mK HFI bolometer, deposit energy produce *glitches* ([Planck collaboration result I](#))^[16] on data. Generally, CRs can interact with each modul of bolometer. Therefore deep understanding and careful data processing of the glitches are necessary. Moreover the result can impact the measurement of the polarization of the CMB. The effect of CRs have been characterized in the *Planck* data, but analytic and modeling of the interaction is needed.

On this report, a simple model of the interaction of primary CRs with the bolometer is developped in order to compute the expected cumulative distribution $N(> E)$ of glitches, the deposit energy and the distribution events of glitches occurring in coincidence in both bolometer couple'. The two dimensions histogram will show the coincidences count in a PSB pair corresponding to deposit energy. Predicted counts are compared to the statistics of events measurement in data.

This work will allow to estimate the effect of long glitches on the polarization of the CMB. The goal is to check if we able to predict the observed distribution of glitches or there are some things contribute on the data which we are do not totally understand such as secondary cosmic rays, solar activity, assumption of model...

Chapter 2

Cosmology, CMB and the Planck satellite

2.1 Cosmology and CMB

The physical cosmology is the branch of the astronomy that deal with the origin and evolution of the Universe as a whole. In the 16th century, Nicolaus Copernicus, the Italian scientist suggested that the Sun is center of the Solar system. In 17th century, Isaac Newton was solved the planetary motion by gravitation force. The modern cosmology was started in 20th century, three century after Isaac Newton, in 1917, Albert Einstein published the theory of gravity in the paper 'cosmological considerations of the General Theory of Relativity'. In 1929, Edwin Hubble's discovered the redshift of the light of distant galaxies, it means that they were rushing far away from the Milky Way with a velocity proportional to the distance. Hence, the Universe must be expanding. Therefore the Big Bang model which suggested by Georges Lemaître in 1927, was accepted. The Big Bang theory described the Universe as a whole and have begun 13.798 ± 0.037 billion years ago. The Universe contains 4.9 % ordinary matter, 26.8 % dark matter and 68.3 % dark energy ([Planck Collaboration 2013 result](#)) [5].

The evolution of the Universe is illustrated in figure 2.1 under the Big Bang theory. The Cosmic Microwave Background (CMB) is radiation from around 380 000 years after the Universe was born. Before this time, the Universe was so hot, dense and opaque that it was made of plasma of matter and energy. Thus photons could not travel freely and no light escaped from those earlier times. The CMB was emitted at the recombination era where electrons combined with p and He nuclei to atoms and photons suddenly free to propagate in all direction. During a small interval time, the Universe suddenly switched from opaque to completely

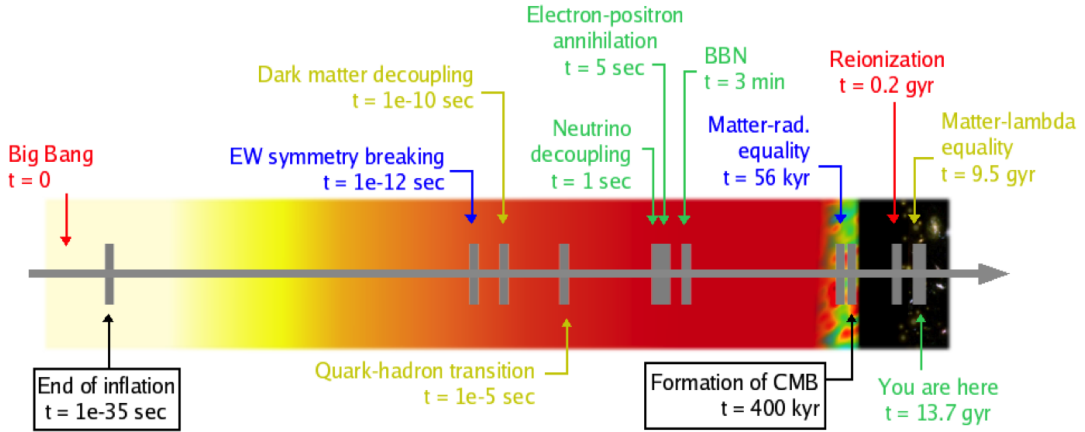


FIGURE 2.1: The evolution of the Universe from the initial singularity to cosmic inflation, quantum gravity epoch, nucleosynthesis, last scattering and present today([Nguyen Trong Hien - Quynhon Workshop](#)).

transparent. The photons were able to travel unimpeded for the entire remainder of the Universe's evolution. This process called as decoupling. Then photons reached us from all direction from the surface of last scattering¹ [15][8]. The temperature of the CMB is not exactly similar in the all direction and contains small anisotropies. The temperature anisotropies originate from metric perturbation in the Universe generated during the inflation phase. CMB anisotropies are contributed from many physical sources. There are some of the primary sources: (i) Gravitational perturbations, there have an intrinsic temperature variation at last scattering surface due to the photon moving out of a gravitational potential and loses energy in the process. Then it links temperature anisotropies and potential fluctuation in the early Universe. (ii) Density perturbations (adiabatic) at the recombination era, the baryonic matter and radiation can be compressed by coupling then the temperature will be increased. This small fluctuations oscillated like sound wave. (iii) the Doppler perturbations, there have a variation in the redshift of the photons when it travel to us... The CMB radiation is polarized due to it was scattered of free electrons during decoupling because of local temperature anisotropic. The polarization pattern can be decomposed into two components: Curl-free component called 'E-Mode' (electric-field) or 'gradient-mode' and Grad-free component called 'B-Mode' (magnetic-field) or 'curl-mode' ([Paolo Cabella and Marc Kamionkowski](#)) [18] [9]. The B-Mode is impacted by gravity waves which is evidenced for inflation theory at the early Universe. CMB power spectrum depend on cosmological parameters. The high accuracy measurements the temperature and polarization anisotropies of the CMB provide us the parameters of density of energy component such as dark energy, dark matter, baryons, parameters of

¹The imaging surface of sphere which photons travel to us since the decoupling happened around at 3000 K

primordial fluctuation spectrum, searching for gravity wave perturbations at the early Universe, detection gravitation lensing by cluster matter.

After billions of years, the Universe has expanded and cooled $T \propto 1/a(t)$ with $a(t)$ is scale factor [15]. Thus the wavelength of the photons has stretched (redshift) into the microwave electromagnetic spectrum roughly 1 millimeter (we can see the CMB on the television) and the CMB temperature has decreased to around 2.7 Kelvin just above absolute zero (-273 K). These photons fill everywhere in the Universe today and create a background that can be detected by far infrared and radio telescopes. Thus observation the CMB allows to studying the physical cosmology at early times and inflation phase.

2.2 The Planck satellite

In 1964, Robert Wilson and Arno Penzias first detected CMB by using a large radio antenna and they got the Nobel Prize in Physics in 1978. The first space mission to detect CMB anisotropies is Cosmic Background Explorer (COBE). In 1989 it was launched by NASA and placed into Sun-synchronous orbit². COBE also measured the CMB temperature and showed that CMB spectrum is a black-body with a very high accuracy at 2.73 Kelvin. The team go the Nobel Prize in Physics in 2006. Studying these tiny fluctuation in more detail, there was other balloon and ground based mission after COBE such as: BOOMERanG experiment 2000 reported that the highest power fluctuation occur around 1^0 , Degree Angular Scale Interferometers (DASI) detected the polarization of CMB and Cosmic Background Image (CBI) presented the E-mode. The second generation space mission, the Wilkinson Microwave Anisotropy Probe (WMAP) was launched in 2001. The *Planck* mission was launched in 2009 to study the CMB with unprecedented accuracy. After measurement the CMB temperature tiny fluctuation by WMAP, the *Planck* instrument measures with high accuracy the temperature power spectrum and mapping all-sky CMB. In addition, It has better angular resolution and sensitivity, the *Planck* experiment will give very interesting constraints on primordial B-Modes which evidence of inflation epoch. For more detail discussion in the *Planck* Scientific Program [12].

²It is geocentric orbit which has the same local mean solar time

The *Planck* satellite is placed at the second Lagrange point (L2) of the Earth-Sun system ³ and entered a Lissajour orbit ⁴ around this point at L2. The gravitational force is balanced, the spacecraft can be maintained to the same relative position with respect to the Sun and the Earth thus calibration and shielding are simplified. L2 provides a stable environment, the satellite will avoid the thermal of the Earth and reached the temperature under 100 K.

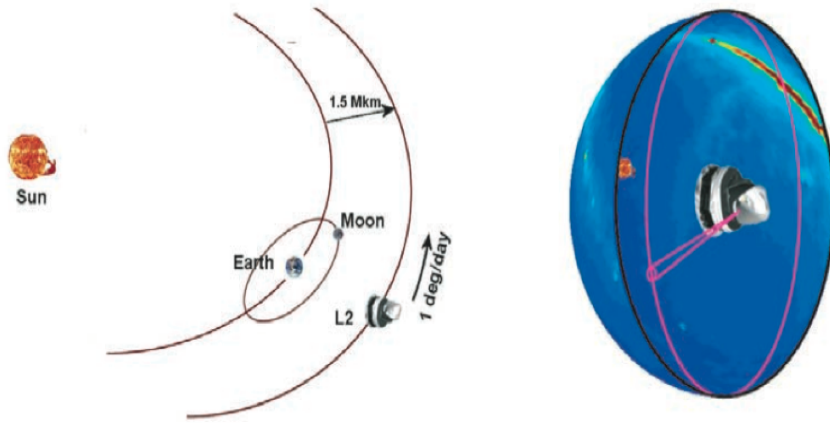


FIGURE 2.2: Diagram of the *Planck* satellite at the second Lagrange point of the Earth-Sun-Moon system. ([Scientific Programme ESA-SCI\(2005\)](#)) [12]

The figure 2.2 shows the spin of satellite $\approx 1^0$ per day follows the Sun. Then the whole sky is observed in 6 month and twice times per year. The design of the spacecraft is such that the spin axis point to the anti-Sun orientation. It helps minimizing thermal fluctuations and cools the payload of *Planck*.

The main components of the *Planck* satellite are showed in figure 2.3. A telescope 1.5 m diameter operate at 20 K and 0.1 k. The Low Frequency Instrument (LFI) observed the sky at three frequency bands centered at 30,44 and 70 GHz detectors are cooled to 20 K. Whereas the High Frequency Instrument observed the sky at six frequency bands centered at 100, 143, 217, 353, 545 and 857 GHz. This is detail in table 2.1. Several frequency bands optimized for removal foregrounds due to dust emissions[12]. Therefore the combination of the two instruments produce the most accurate map of the CMB anisotropies. The *Planck*'s telescope

³The distance

- Sun-Earth: 1 AU = 150 million km.
- Earth-Moon: 384 000 km.
- Earth-L2: 1.5 million km

⁴Lissajous orbit are the natural motion of a satellite around a co-linear libration point in a two-body system and require less momentum change to be expended for station keeping than halo orbits, where the satellite follows a simple circular or elliptical path about the Lagrange point 2.

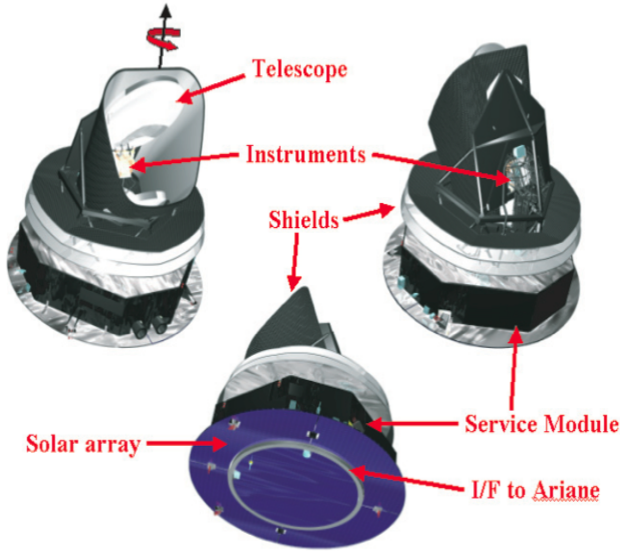


FIGURE 2.3: The main components of *Planck*: Telescope, HFI, LFI instrument detector, the Solar array is always exposed to the Sun, the Service Module contains all warm elements of the satellite and cool the telescope and instrument, and the shield protect the spacecraft from solar radiation([the scientific Programme ESA-SCI\(2005\)](#)) [12].

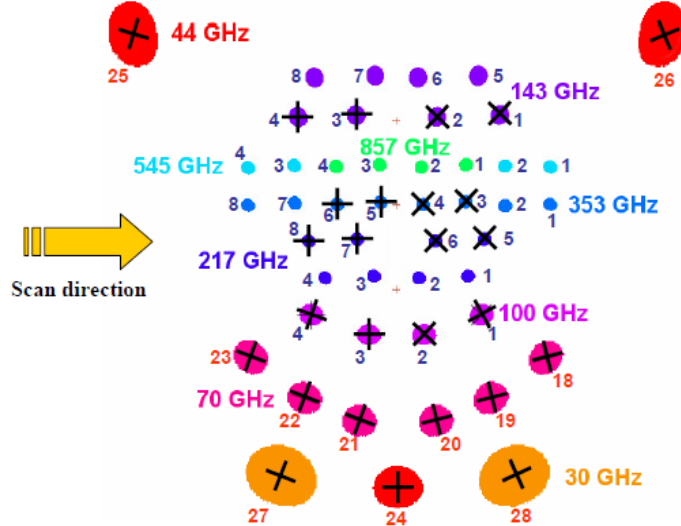


FIGURE 2.4: The Planck focal plane with direction of scanning. The polarization sensitive bolometers with crosses indicate the direction it possible to measure Stokes parameter I, Q and U([Planck pre-launch.](#)) [11, 20]

collects radiation from the sky and delivers it to a focal plane populated with 70 detectors. There are two kinds of detectors: wideband bolometers operating in the 90 -1000 GHz, and low-noise amplifiers operating in the 20 - 80 GHz band (figure 2.4). The detectors are stable, sensitive and fed by radiation in feedhorns ([X. Dupac and J. Tauber](#)) [21]. The *Planck* focal plane scans the sky in small angle from 85° up to 89° and spins at a rate of 1 rotation per minute therefore the

Planck observation strategy is 1 measurement every 5 ms and 1 cycle per minute ([Planck Explanatory Supplement](#))[\[11\]](#).

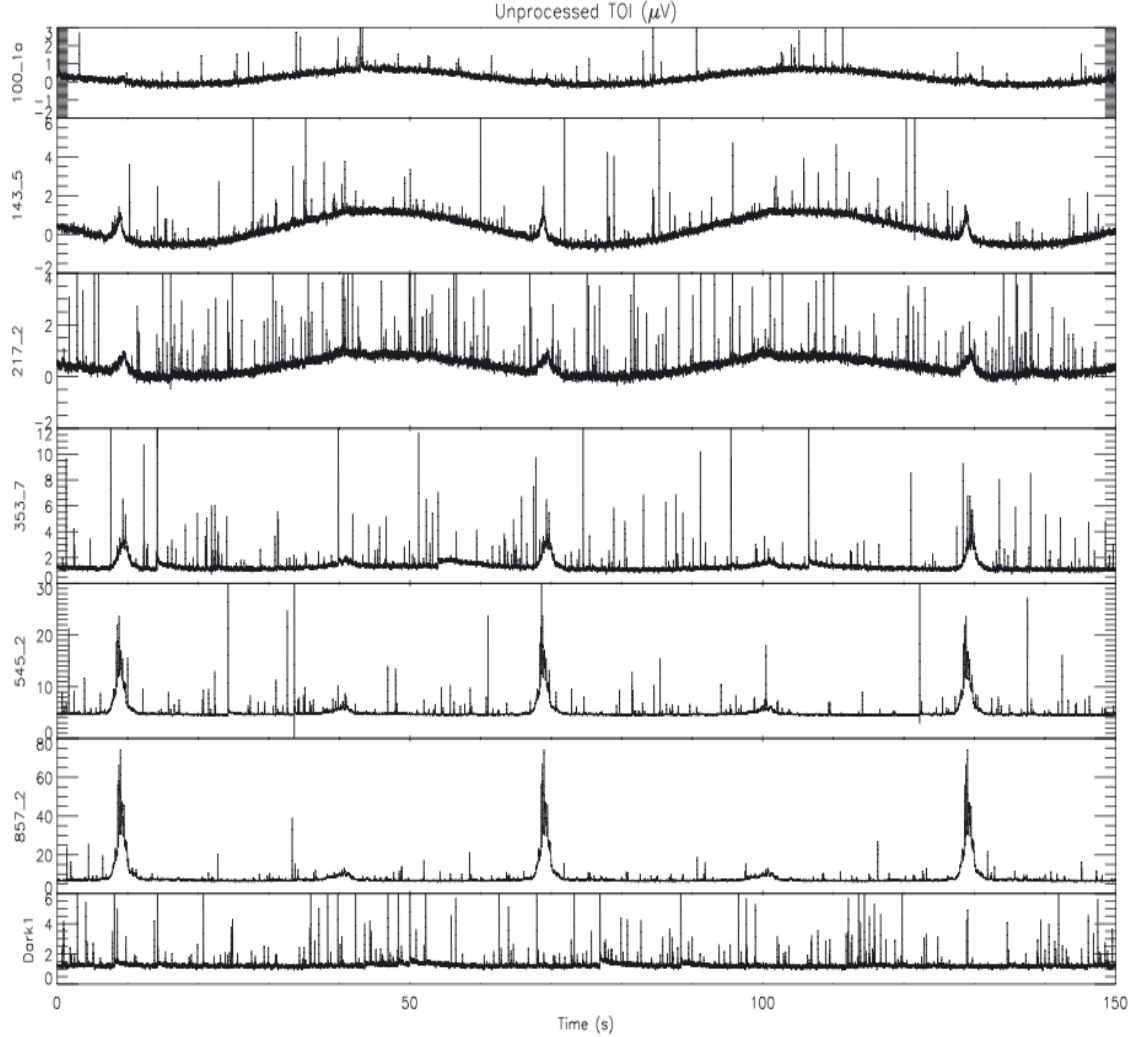


FIGURE 2.5: The raw data (unprocessed) of six frequency band and one dark bolometer show in time (> 2 cycles). The time order information (TOI) is dominated by the CMB dipole, the Galactic dust emission and glitches. The rate of glitches are quite conspicuous([Planck early results.IV.](#)) [1, 10]

The *Planck* data was taken from August 2009 to the end of 2011. The *Planck* satellite controlled from the Mission Operations Center (MOC) in Darmstadt - Germany. Scientific data sent daily from MOC to Data Processing Centers (DPCs). The DPCs are responsible for all levels of processing of the *Planck* data. Figure 2.5 shows the raw data of six HFI frequency: 857, 545, 353, 217, 143, 100 GHz and one dark bolometer in 150 seconds. It indicates that the data is dominated by CMB dipole, Galactic dust which absorbed in mm wave length and *glitches*. The contribution of glitches rate which are produced by cosmic rays, is clearly visible and require careful data processing. On this report, the work will

allows us to improve our understanding of glitches, in order to better quantify the impact. ([the scientific Programme ESA-SCI\(2005\)](#) [12]).

2.2.1 The HFI bolometer

HFI combines spider-wed bolometers (SWB) and polarization sensitive bolometers (PSB) cooled to 0.1 K in order to minimize sources of noise and effect of cosmic rays for the measurement of the CMB fluctuations with angular resolution to 5 arcminutes.

TABLE 2.1: The HFI bolometers

Band	Frequency (GHz) center	Quantity	Angular resolution (arcminutes)
100p	100	8	9.5
143p	143	8	7.1
143	143	4	7.1
217p	217	8	5.0
217	217	4	5.0
353p	353	8	5.0
353	353	4	5.0
545	545	4	5.0
857	857	4	5.0

p: stand for polarization

A bolometer detects millimeter wavelength and infrared light by measuring the heat caused by photons absorbed by the crystal. photons are absorbed by a grid (like a spider wed) (figure 2.6). The increasing temperature is measured by a tiny thermometer in the center of the detector. The change of the temperature depends on the intensity of the coming light. Bolometers detect any source of heat including cosmic rays which can penetrate the bolometer and deposit energy. SWB bandwidth is selected by filter, is designed to absorb long-wavelength thermal radiation therefore the high energy particles pass through. The SWB consists of micron thick silicon nitride, covered with gold. The shape of the thermistor is 30x100x300 μm at the center (figure 2.6 bottom). The SWB grid and diameter varies depending on the frequency bands. [1]

Planck HFI has 32 PSBs which can measure the polarization of incoming light. Instead of a circular SWB, a PSB consists of a grids which allows only absorb a single polarization of the electrical field of incoming radiation. Specially, the PSB is worked in a pair (PSBa and PSBb) with perpendicular orientation place on the top of each other thus each linear polarization is detected simultaneously. The bolometers are mounted on a copper-plates stainless steel plate called housing module cooled down to 0.1 K and fluctuations of a few microkelvin (figure 2.6 top).

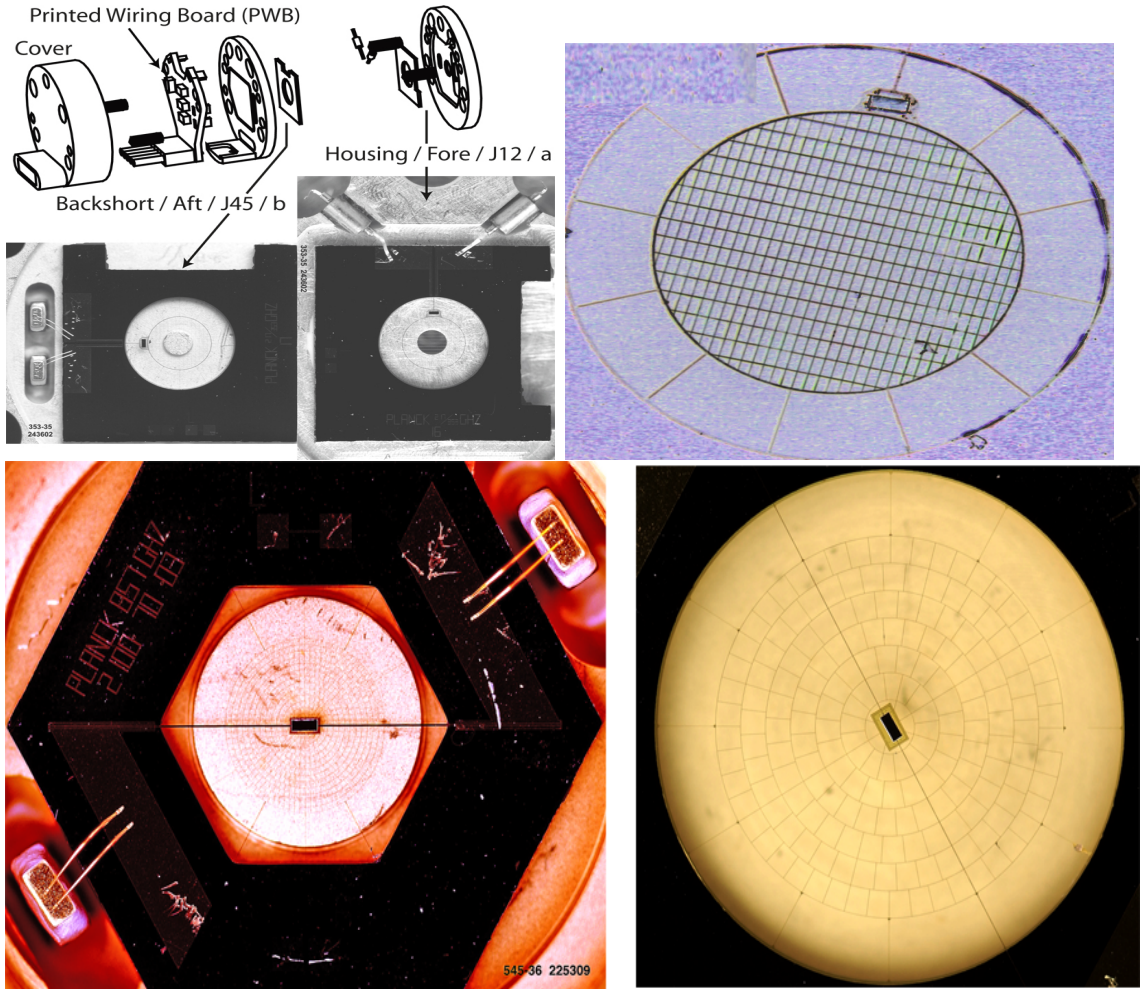


FIGURE 2.6: *Top left:* Bolometer PSB pair (a and b). *Top right:* The parallel grid of PSB and thermometer on the edge. *Bottom:* The spider wed bolometer with the thermometer placed at the center [17].

Four couples of the PSB allow to detect linear combination of the Stokes parameters I, Q and U. Q and U are linear polarization parameters in each four bands (100p, 143p, 217p and 353p GHz).

2.2.2 Components of the HFI bolometer

As described before, HFI detectors are assembled by using silicon nitride (Si_3N_4) and neutron transmutation doped (NTD) germanium thermistors with resistances. We now described the different components of the detectors:

- *Thermometer:* It is a NTD germanium semiconductor. It has the same size between PSB and SWB: $100 \times 300 \times 30$ (thickness) μm .

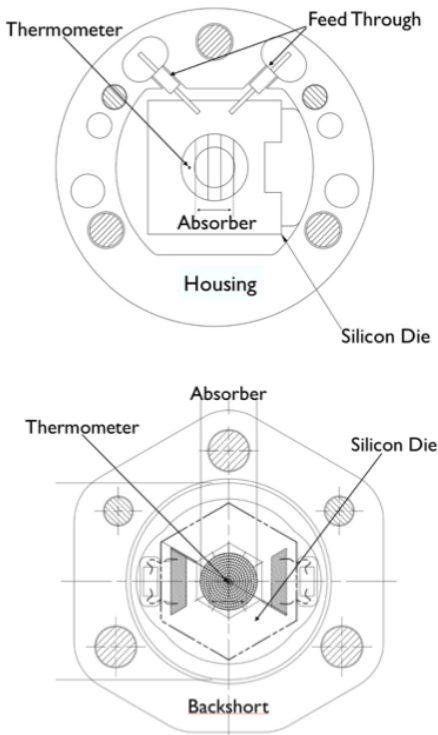


FIGURE 2.7: *Top and bottom:* A perspective drawing of a PSB, a SWB and the components [10]

- *Absorber:* It absorbs the millimeter wavelength both PSB and SWB. It is composed of a micro mesh of Si_3N_4 , the size of micro mesh depends on the HFI frequency bands and ranges from 5 to 10 μm with 1 μm thickness. It allows to reducing the cross section of CRs and shorter photon wavelength. The grid space of PSB is greater than 50 μm thus It absorbs millimeter wavelength.
- *Silicon Die:* The size of wafer is between 0.4 to 0.8 cm depending on the frequency bands and the thickness is 350 μm for all the bolometers. The shape is different for PSB and SWB (figure 2.7), the geometry on PSB can be approximately as square and hexagon on SWB.

- *Backshort:* It supports the silicon die and it optimizes the absorption of the photons by the grids.
- *Cover:* It protects the PWB and supports a connector.
- *Housing:* It made of beryllium-copper (CuBe) and supports the silicon die of the PSBa bolometer.
- *Printed wiring board (PWB):* The PWB is assembled in the bolometer module on the opposite site of the backshort. It contains surface mount inductors and a ground plane, forms with capacitors and bolometer filter to attenuate radio frequency signal before it is rectified at the bolometer [6, 10]. For more detail, we can see figure 2.6 *top*.
- *Feed through:* It is placed in the forward of a PSBa. It links a bolometer with PWB.

Chapter 3

Cosmic ray, interaction with detectors

3.1 Cosmic rays

What are Cosmic Rays (CRs) ? At the start of the 20th century, scientists interested in a puzzling phenomena. There was indication of a radiation from the outer space. In 1909, Theodor Wulf developed a device to measure the rate of ion production from the top of Eiffel tower he showed an excess of radioactive as compared to inside a container. However his publication was not widely accepted. In 1912 the puzzle was solved by Victor Hess, a German scientist. He used a gold leaf electroscope for radiation counter on a balloon flight to 17500 feet (1 ft = 0.305 m) high which made his life risked. The increasing amount of radiation demonstrated that the radiation exists from outer space and is named 'Cosmic Radiation'.

How do we study CRs ? It depend on the level energy. The low energy CRs are absorbed in the top of the atmosphere then they are only detected by instruments in spacecrafts. The high energy cosmic rays create a shower particle in atmosphere (20 km), the Cerenkov radiation is detected by telescopes on the ground.

Where are Cosmic Rays produced? The origin of CRs is still a question in high energy astrophysics. However the places in the universe where such high energy $> 10^{18} eV$ is produced either have huge magnetic fields or have gigantic size. Thus it can be produced from interstellar mediums or supernovas, pulsars, active galaxies. Therefore, cosmic rays are relativistic particles traveling through our Galaxy and in the Solar system. CRs at the second Lagrange point origin from many sources (Galactic, the Sun, stars, supernovas, pulsars, active galaxies

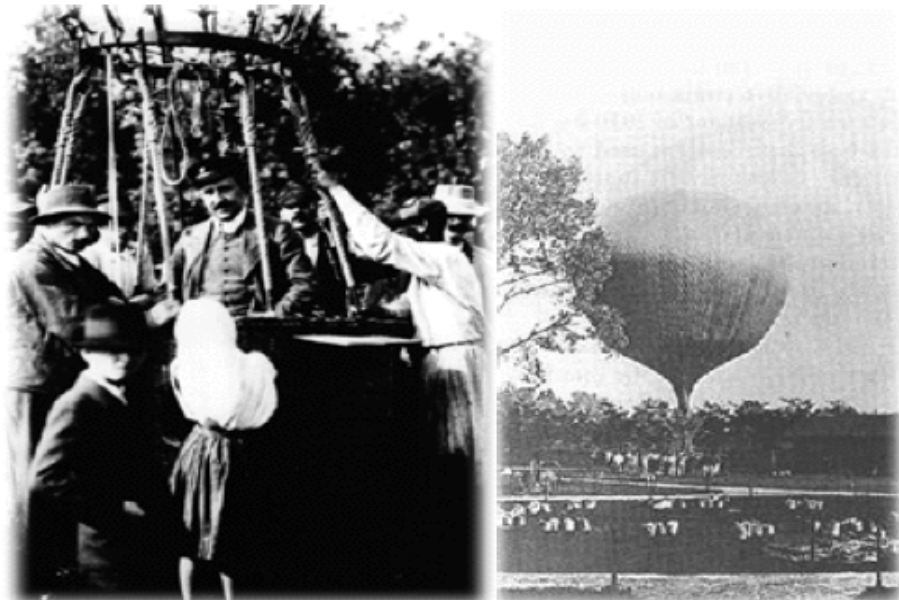


FIGURE 3.1: Victor Hess (*left center*) and his balloon before flight. He observed cosmic rays by increasing altitude of a gold leaf electroscope.

...) Including 89 % proton, 10 % α -particle 1 % nuclei of heavier elements and electrons. There is a small fraction of heavier particles, about 0.25 % , which are light element (lithium, beryllium and boron) ([R.A.Mewaldt et al. 2010](#)). But there are evidence that these light elements have been produced by primary cosmic ray particles like protons collision with carbon and oxygen in the interstellar medium. Likewise the medium elements between silicon and iron have been supplemented by cosmic ray spallation ¹ known as secondary cosmic rays. The Planck satellite is effected by mainly proton and Helium from MeV to 10 GeV. Figure 3.2 show the energy spectrum of the components of the cosmic rays, there is high abundance of proton and Helium. The ratio of secondary to primary nucleic deceases with energy.

The main contribution of CRs is from the Milky Way Galaxy. The high energy charged particle are modulated by the solar wind and solar activity for particles with energy less than 10 GeV ([R.A.Mewaldt et al. 2010](#)). [2]

Secondly, the Sun is a source of CRs, nucleic and electrons that are accelerated by magnetic field of solar flares and shock-waves. Typically the energy of the solar particle the order of keV. Those low energy particles do not reach bolometers, so except during flares, only galactic particles affect the data. Additionally the maximum energy of a solar flares can reached 10 to 100 MeV. We observed 13 solar flares during the *Planck* mission each of it lasted a few hours and affect on change the temperature of the whole bolometers focal plane. Thus there is 1 GeV

¹The CRs impact with matter and formation the elements

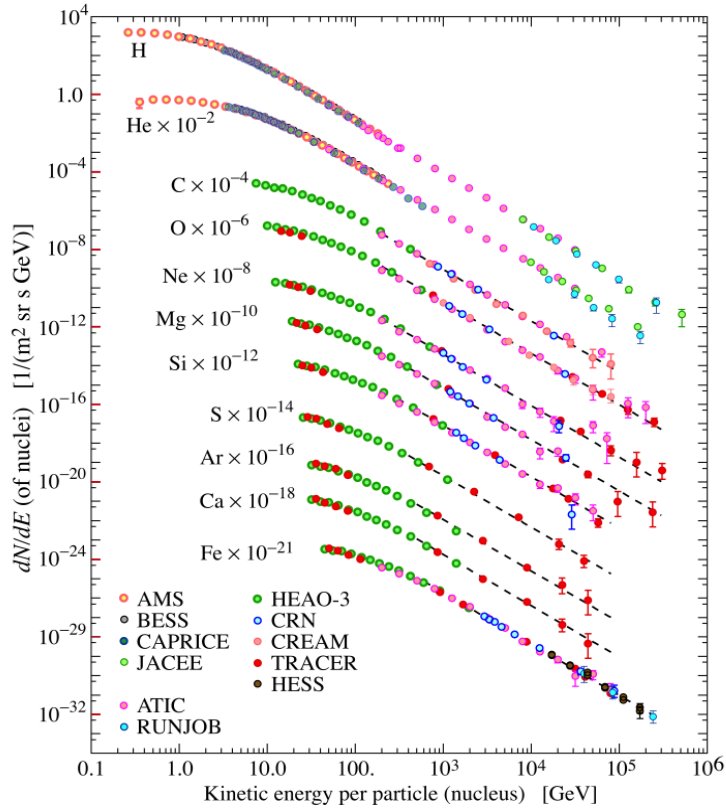


FIGURE 3.2: The spectrum of particles per energy-per-nucleus. The figure was created by P. Boyle and D. Muller ([L O'C Drury](#)) [3]

for a year and 10 GeV for a decade. The data of these events are excluded by standard HFI data processing, then we will not mention this source of CRs on this report ([A.Catalano et al. 2014](#)). [10].

There is also a population of *Anomalous cosmic rays* (ACR). There are mostly emitted by neutral atoms in the interstellar medium (ISM) which leak into the heliosphere, get ionized by the solar ultra violet radiation or charge exchange with the solar wind, accelerated by the solar wind termination shock. In ACR there have more helium than protons and much more oxygen than carbon. This can be explained by predominantly neutral in the interstellar medium. The energy of protons are between hundreds of keV and 100 MeV then it is a marginal component of the cosmic rays flux effecting the *Planck* HFI ([A.Catalano et al. 2014](#)). [10]

On the *Planck* satellite, the flux of CRs are monitored onboard by the Standard Radiation Environment Monitor (SREM)². Solar flares provided useful tests to correlate the signal measured on the outer space of satellite with SREM. We found that the CRs with energy below 39 MeV can not penetrate the focal plane unit.

²SREM is a particle detector, developed by the European Space Agency for space applications. It measures hight energy proton (from 10 MeV to 300 MeV) and electrons (from 300 keV to 6 MeV). It consists of three silicon detector (D1, D2 and D3) ([A. Mohammadzadeh et al.](#)) [7]

Thus the low energy particles can not penetrate the material of the satellite and interact with bolometers.

Finally, the high energy particles that can produce glitches in the HFI data is in a range of 39 MeV and 10 GeV including primary particle protons and helium. Moreover the flux of protons around 200 MeV are showed in the figure 3.2, and is $3000 - 4000$ particles $m^{-2}sr^{-1}s^{-1}GeV^{-1}$. The shape of spectrum is power law with index ≈ -3 and in the Cosmic Ray field, these features are usually referred to as the 'knee' and the ankle.(O.Adriani, G.C. Barbarino et al.2011) [4].

3.2 Interaction of cosmic rays with the detectors

There are different ways for a particle interact with mater. For example, the charge particles can change the direction, collision with electrons or nucleic ... If the charge particles travel in material, it will have certain probability to interact with the nuclei or with the electrons in the material through the electromagnetic force. This probability depends on the thickness, the number of particles in the volume and the nature of the interaction. However, there are two main way interaction of energetic particles with matter: ionization and nuclear scattering. The ionization is the main effect to deposit energy, when the energetic particles penetrate material, it collision with atoms or sub atomic particles and produce electrons excited. The result is atoms acquire positive or negative charge by losing or gaining electrons.

The *Planck* is impacted by primary CRs proton and Helium and heavier elements interacting with detector as well as satellite at the second Lagrange point. When CRs penetrate on the material of detector. It will deposit energy in the components. If the energy of particle is small enough it will be totally absorbed. When high energy particle interact with material, It will produce the secondary particle at lower energy. It can be a shower therefore increasing the deposited energy.

Figure 3.3 shows three family of glitches and a PSB. The *short glitch* is result from primary CRs hitting the thermometer or grid of absorber. Due to the fact that the geometry of thermometer is $30 \times 100 \times 300 \mu m$ and typical energy of Galactic protons around is 1 GeV, then the energy loss $\approx 1.47 \text{ MeV } cm^2 g^{-1}$ ([Planck Collaboration I 2013](#)) [17]. The *long glitch* are produced by CRs hitting the silicon die (section 2.2.2). The ground base tests indicated that the thermometer is sensitive with the temperature change of the silicon die ([A. Catalano et al.](#)) [10]. It has been show that CRs impacting on Si die produce the temperature rise and falling with the fast rise time and slow tail are produced as the heat conducts.

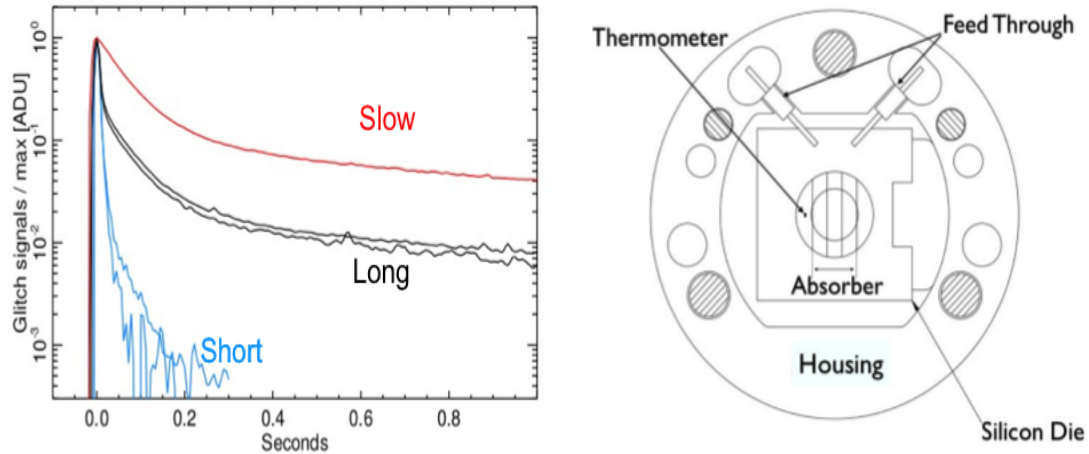


FIGURE 3.3: Three family of glitches for PSB on raw data. The glitch rate is 1 per second. Short glitch time response is 0.2 s and the tail is small enough to affect to the data. Long glitch is long events (rise time 0.35 to 0.5 s) and the slow tail has long time constant. Slow glitch are detected only on PSBa, the slow tail has rise time similar the long glitch and they can fit accuracy by a simple linear function. (Planck Collaboration I 2013) [17].

The tail has time constants of the order of 50 ms, 500 ms and 2 s for PSB-a, 35 ms, 500 ms and 2 s for PSB-b and SWB. The raw data show that the rate is about 2 glitches per second. The dimension of Silicon die is from 0.4 cm to 0.8 cm and thickness $350 \mu\text{m}$, thus understanding characterization and remove the effect of the long glitches on the *planck* raw data play a vital role for science analysis. To summarize, the loss energy will contribute thermal by conductance and capacitance. Thus it will effect on raw data of the *Planck*.

3.2.1 Interaction with the silicon die

In this report, we focus on the interact of CRs with the silicon die as those events are the most problematic for data analysis. The *long glitches* are clearly produced by CRs interaction with the silicon die in raw data. But, how it happen?. In general, there are two principal feature characterizing the travel of charged particle through silicon die: amount of deposit energy and deflection the incident particle. These effect are primarily processed through inelastic collision with the atomic electrons of the Si and elastic scattering from nucleic.

Figure 3.4 shows the CRs interaction with Silicon die. There have two ways when incident particles through inside Si. The charge particles will be deflected by elastic collision. This reaction do not modify the nature and the coming energy of the initial particles then kinetic energy is conserved. The nonelastic collision produced secondary particles and the kinetic energy is not conserved then the main

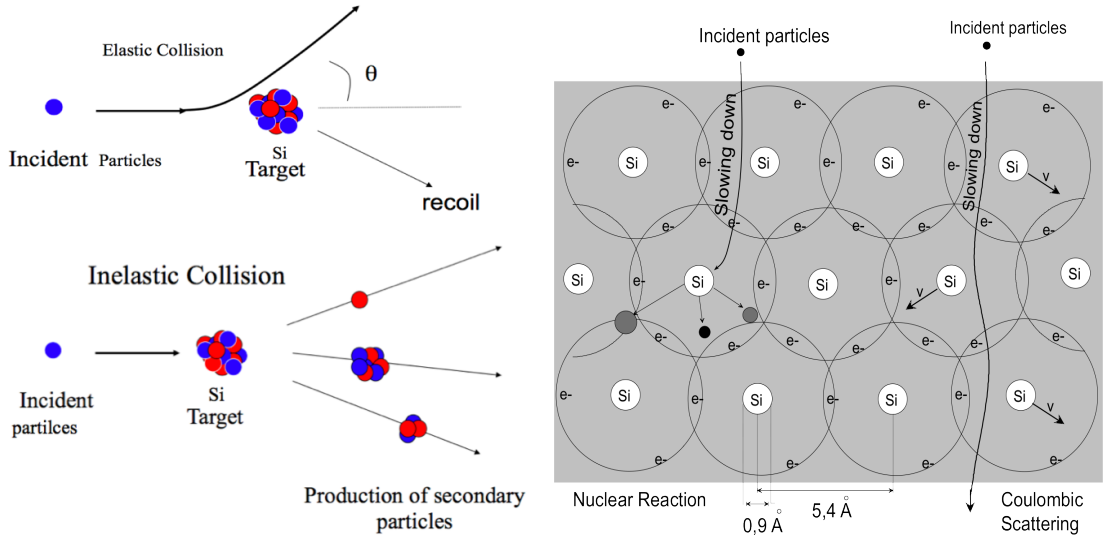


FIGURE 3.4: The CRs penetrated into Silicon die. The main processes is elastic by electromagnetic force and reaction with nucleic of Si.

effect is ionization and displacement. Both processes lead to loss of energy and can be produced electrons, positrons. They will impact with silicon die following many processes as Bremsstrahlung, Cerenkov light or annihilation... ([William R. Leo - 1987](#))^[14] Eventually, the deposit energy can increase, then the temperature of the silicon die will rise.

The total energy loss can be described by the stopping power of material. This is the evidence of the *long glitches* on the Planck raw data. Figure 3.5 as an example, shows the stopping power of *muons* particle through copper of energy range MeV, GeV and TeV. The minimum ionization particles is at $\beta\gamma = p/Mc \sim 3$ ³. The deposit energy of CRs hitting on silicon die have a similar shape that the solid curve in the figure 3.5.

The deposit energy will induce temperature variation of thermometer ($E \sim k_B T$) and effect on the *Planck* signal. Figure 3.6 shows cumulative distribution ($N > E$) of long glitches for several bolometers per unit of surface per hour by the *Planck* experiment. In the next part, I will model the interaction in order to explain the observed shape.

³p: momentum of particle, M: mass of particle, $\beta = \frac{v}{c}$, $\gamma = \frac{1}{\sqrt{1 - \beta^2}}$

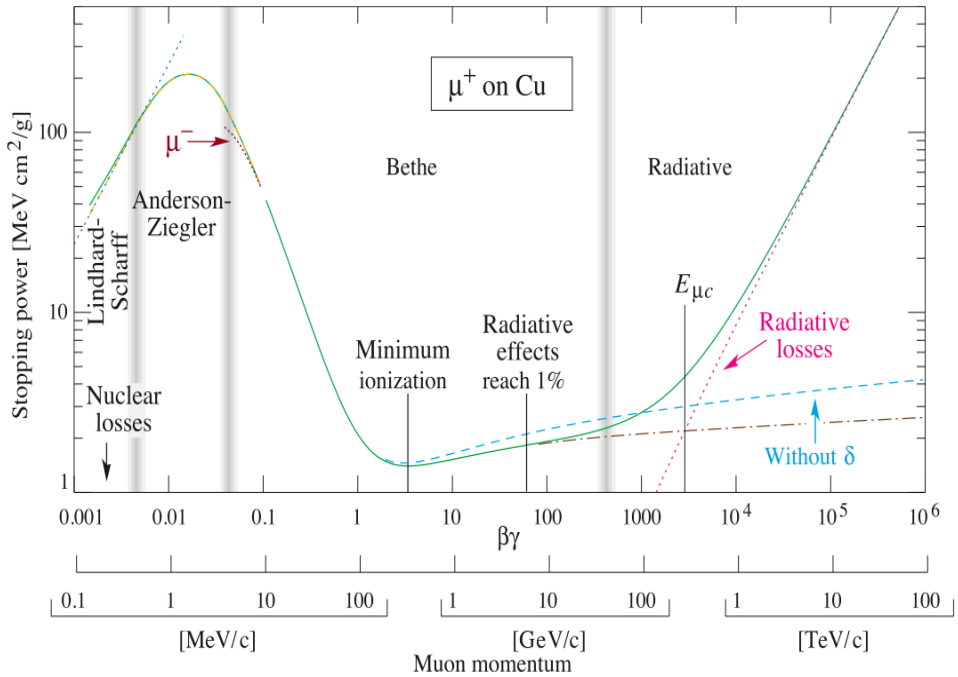


FIGURE 3.5: Stopping power of positive muons in copper. The solid curve indicate the total stopping power $\text{MeV } \text{cm}^2 \text{g}^{-1}$. The horizon axis is function of $\beta\gamma$ and range energy.(J. Beringer et al. (Particle Data Group), Phys. Rev. D86, 010001 (2012)).

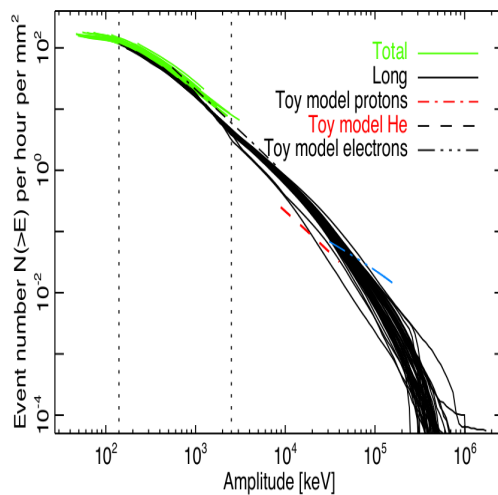


FIGURE 3.6: The long glitches of the experiment data was public on the *Planck* result (Planck Collaboration I 2013) [17].

Chapter 4

Methodology

In this chapter, I will model and simulate the flux of particle respect with energy deposited in the silicon die per unit of time to reproduce the observation spectrum of the long glitches as well as coincidences of the long glitches between the two PSBs.

4.1 The simple modeling

We assume a CR coming with energy E_0 , the angle θ and hitting the silicon die. The energy range is between 1 keV and 10 GeV for the input energy spectrum. We have also assumed uniform distribution of angle θ . This is not a very good assumption around the bolometer because different components in the satellite and in particular around the bolometer absorb the energy of incoming particles...

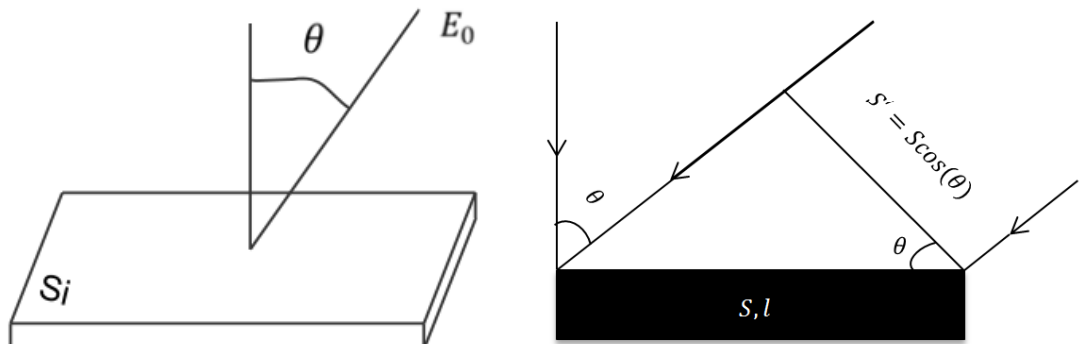


FIGURE 4.1: The simple model of the coming particle with the angle and the surface change

We assume energy distribution of incoming particles $\frac{dN}{dE_0}$ are given by the PAMELA experiment (a Payload for Antimatter Matter Exploration and Light-nucleic Astrophysics)¹ as shown in figure 4.2. The figure shows the spectrum of cosmic rays per unit area per time per GeV for each nucleic [4].

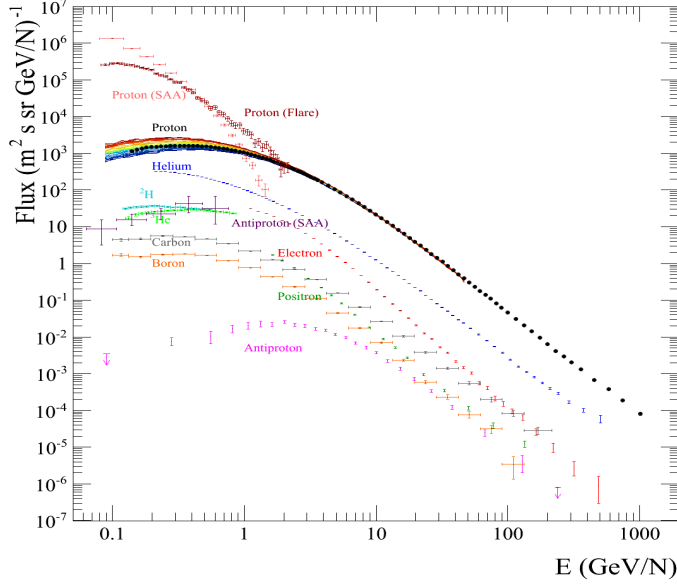


FIGURE 4.2: The PAMELA result for flux of particles per GeV ($\frac{dN}{dE_0}$)

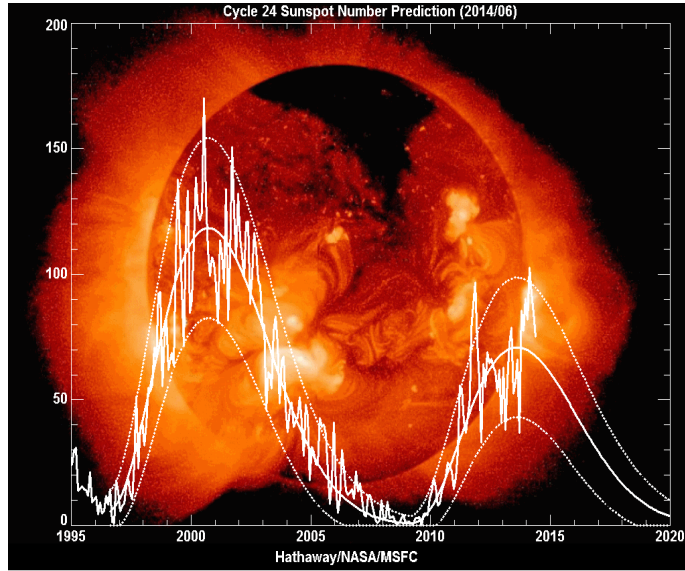


FIGURE 4.3: The solar sunspot in 11 years from 1985 to 2015 experiment and prediction (Dr. David Hathaway et al.)[13]

¹PAMELA was launched June 2006 by rocket Soyuz from Baikonur in Kazakhstan. The satellite is traveling around the Earth at Low Earth Orbit range 350 - 610 km with inclination 70°

We also have to account for the sun activity. Solar activity rise and fall with a cycle about 11 years. Emissions of matter and electromagnetic fields from the Sun decrease during low solar activity, making it easier for Galactic cosmic rays to enter the Solar system. Therefore CRs intensity is higher when solar activity lower [19]. Figure 4.3 indicates that the Sun activity cycle 24. The vertical shows the number of sunspot while the horizon is the time between 1985 and March-2014. We can see that the number of sunspot during the PAMELA experiment (2006) and the *Planck* experiment (2009) are different several time. Therefore the cosmic rays intensity of the *Planck* mission is higher. Additional the ratio of protons and α particles is between 10 and 20[2].

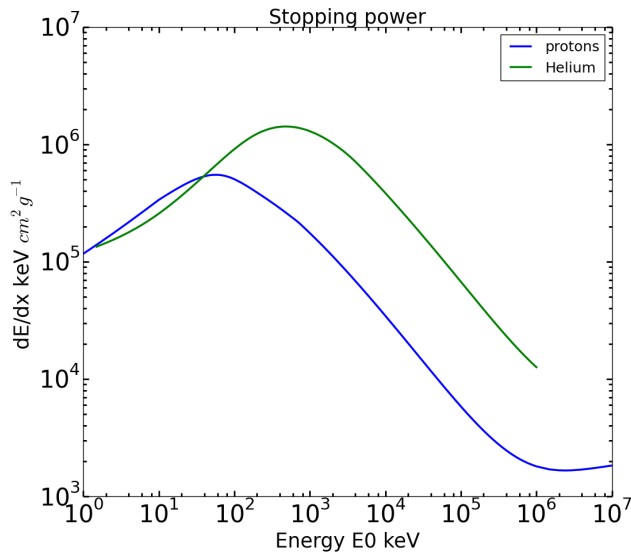


FIGURE 4.4: The stopping power of primary cosmic rays penetrated on the silicon die of the Planck satellite

Because the silicon die have thickness l and the high energy particles come form all direction then we will simply consider the limitation of the angle as $\theta_{max} = \frac{\pi}{2} - \frac{l}{\sqrt{S}}$ and the surface change $S' = S \cos \theta$, this is an approximation since the silicon die is not square and has a hole in the middle. Typically the primary component of CRs are charge proton and α particles, the interaction with matter is described by stopping power ($\frac{dE}{dx}$) as mentioned on the section 3.2. Finally we can calculate the deposit energy through thickness $\frac{dE}{dl} = \rho \frac{dE}{dx}$, with $\rho = 0.002329 g.mm^{-3}$ density of silicon (^{14}Si). Figure 4.4 shows the stopping power of proton and α particle through silicon die of PSB. We see that the curves shapes similar to the one the figure 3.5. However the energy relevant range for the interaction with Planck detectors is from 1 keV to 10 GeV. The α particles have to refine at the minimum $dE/dx \approx 200$ keV, then I miss a few percent of energy.

4.2 Analytical approach

The analytical approach allows us to compute the deposit energy for a bolometer. The primary CRs protons and He coming to the wafer and interact with Silicon die in range of energy E_0 and each angle θ .

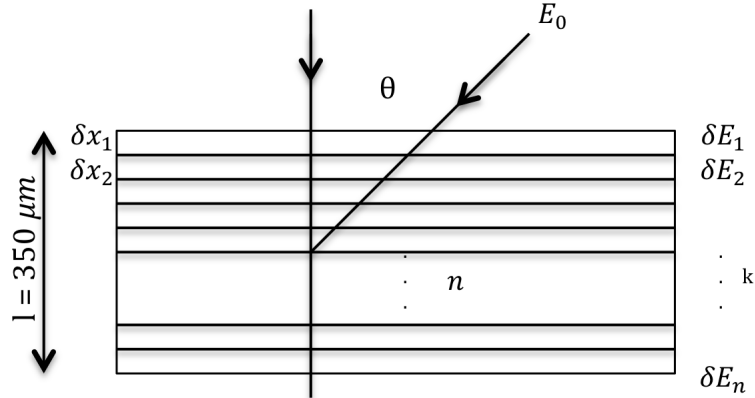


FIGURE 4.5: Deposit energy through n layer of silicon die base of stopping power

We decompose the wafer in n layers in thickness l (μm) of the silicon die. Then each layer has $\delta x = \frac{l}{n} (\mu m)$ as figure 4.5. On the other hand, the particles come from all direction then we have to account to length of particles through inside the silicon die change when particles come from different direction: $\delta x = \frac{l}{n \cos \theta}$. Finally, we compute losses energy through layers:

$\delta E_1 = \frac{\rho l}{\cos \theta} f(E_0)$ where: $f(E_0)$ is stopping power of CRs with silicon corresponding coming energy E_0 (figure 4.4).

$$\delta E_2 = \frac{\rho l}{\cos \theta} f(E_0 - \delta E_1)$$

$$\delta E_3 = \frac{\rho l}{\cos \theta} f(E_0 - \delta E_1 - \delta E_2)$$

.

.

.

The total deposit energy can be approximately computed as:

$$E \approx \delta E_1 + \delta E_2 + \dots + \delta E_n = \frac{\rho l}{\cos \theta} \sum_{j=1}^n f(E_0 - \sum_{k=0}^j \delta E_k) \quad (4.1)$$

The different values of E_0 , can give the same we can have several values of deposit energy E as the stopping power function is not a monotonic function.

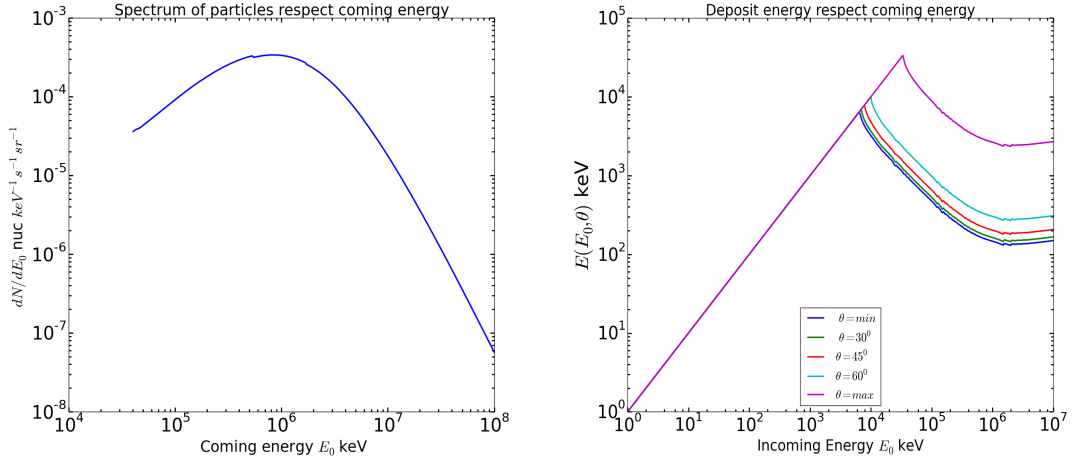


FIGURE 4.6: *Left:* Flux of particle with coming energy $\frac{dN}{dE_0}$. *Right:* Deposit energy with different angles $\theta = \theta_{min} = 0, \frac{\pi}{6}, \frac{\pi}{4}, \frac{\pi}{3}, \theta = max$.

Figure 4.6 shows the number of particles per coming energy $\frac{dN}{dE_0}$ with $E_0 > 39 MeV$. Besides of it, the figure turn out the deposit energy per income energy $E(E_0)$ for different angle $\theta = \theta_{min} = 0, \frac{\pi}{6}, \frac{\pi}{4}, \frac{\pi}{3}, \theta = max$.

The relationship between the number of events per unit deposited and incoming energy for a given θ is then:

$$\frac{\delta N}{\delta E} = \sum_i \frac{\delta N}{\delta E_{0i}} \frac{1}{\left| \frac{\partial E}{\partial E_{0i}} \right|} \quad (4.2)$$

, where we have summed over incoming energies giving the same $E(E_0)$.

The term deposit of energy per coming energy $\frac{\partial E}{\partial E_0}$ is done by derivation the deposit energy through silicon die $E(E_0)$. We have to sum since the deposit energy $E(E_0)$ is not a monotonic function. Different values of coming energy E_0 can give the same value of the deposit energy E .

Finally, We will derive the flux of particle per deposit energy by integrating over angle, energies and consider the surface change:

$$\frac{dN}{dE} = \int_0^{2\pi} \int_0^\pi \sum_{possibility} \frac{dN}{dE_0} \frac{1}{\left| \frac{\partial E}{\partial E_0}(E_0, \theta) \right|} \cos \theta \sin \theta d\theta d\varphi \quad (4.3)$$

The equation 4.3 is calculated flux of CRs per deposit energy per hour per unit surface $\frac{dN}{dE}$. We compute the cumulative distribution function per unit of time

per unit surface area of the Silicon die. Thus we have:

$$N(> E) = \int_E^\infty \frac{dN}{dE} dE \quad (4.4)$$

The primary CRs particles are proton and Helium, thus each term will be compute from equation 4.3 and 4.4.

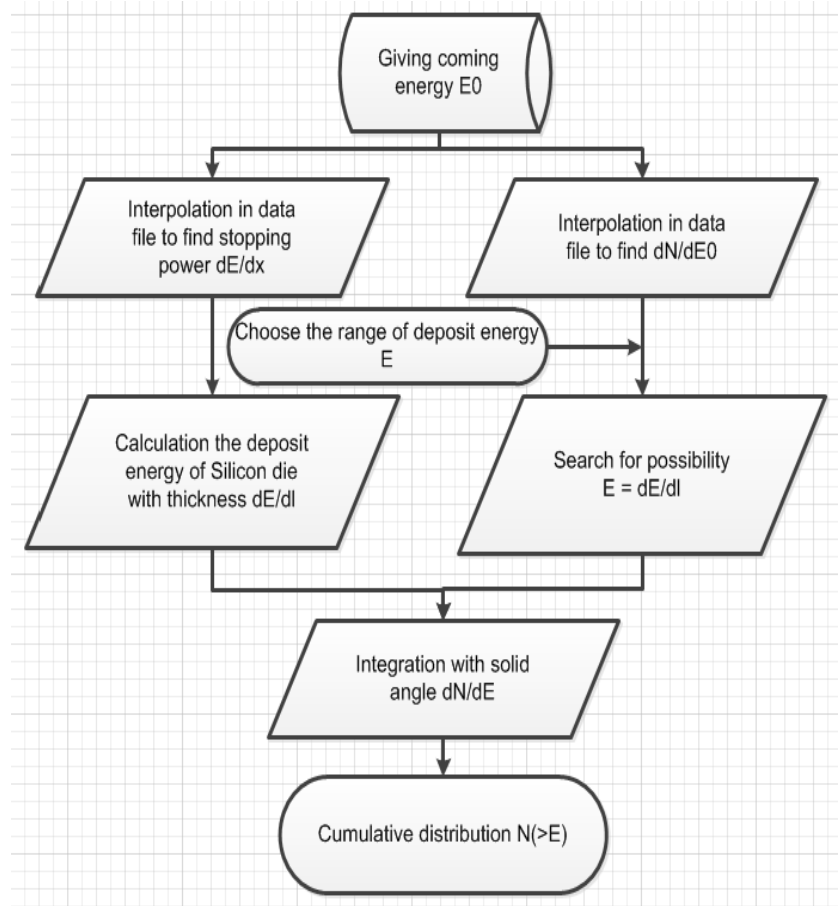


FIGURE 4.7: The flow chart of analytical approach for numerical method

Figure 4.7 indicates diagram of the analytical approach in order from top to bottom. At the beginning, the range of coming energy E_0 are given. As shown on the left hand of the diagram, we compute the deposit energy of CRs through the silicon die. On the other hand, the flux of particles per coming energy $\frac{dN}{dE_0}$ are computed. After that, we search for possibility because many values of coming energy E_0 can deposit same energy E . Finally, we compute the flux of particle per deposit energy $\frac{dN}{dE}$ and cumulative distribution $N > (E)$ of a long glitch. The result will be shown in chapter V.

4.3 Simulation approach

Here we have developed another approach based on simulating the interaction of particles at L2 coming to the silicon die of PSB-a and PSB-b. This approach will allow us to compute more easily the energy deposited in more complicated geometries of detectors, and how event coincidence between PSB pair. The method is the following:

- Loop over the coming energy $E_{0n}, n = 1, 2 \dots n$. Draw particle arrival generated randomly in the sky by a Poisson distribution,² with number of particle coming on the bolometer is $\Delta N = \lambda = 4\pi \frac{dN}{dE_0} \Delta E_0 \Delta S \Delta t$. 4π is coming from the integration over solid angle, ΔS is the surface of silicon die, Δt is the integration time, ΔE_0 is choose corresponding with $\frac{dN}{dE_0}$.
- For each particles with energy E_0 generate an angle θ in the sky, assuming $\cos \theta$ is a uniform distribution, as it should be for isotropic distribution on the sky.
- Account for the effective surface $\Delta S' = \Delta S \cos \theta$ by rejecting a fraction of particle drawn randomly, falling outside the solid angle of the wafer.
- Compute the deposit energy E for each particles with corresponding angle by equation 4.1 (figure 4.8).
- Make the histogram of the deposit energy and get number of particles interacted with silicon die and compute the number of particles per deposit energy $\frac{dN}{dE}$ and cumulative distribution ($N > E$).

Figure 4.8 shows the spectrum of deposit energy events of the PSB-a and the PSB-b for primary CRs protons and Helium in the different range of angle in integration time $\Delta t = 1$ hour. The spectrum indicates that the deposit energy is dominated from $10^2 keV$ to $10^3 keV$ for protons and $10^3 keV$ to $10^4 keV$ for Helium. The low energy is absorbed on the first silicon die and there are some events that the particles deposit significant energy in the first silicon die and absorbed in the second silicon die. The energy deposition events is populated around 1 GeV coming energy E_0 and it is lose much more when the range of angle θ is larger. The shape of spectrum is similar with figure 3.5.

²The property probability of a average number of events occurring in a fixed interval of time and/or space $f(k, \lambda) = \frac{\lambda^k e^{-\lambda}}{k!}$; $e = 2.71828\dots$, $k = 0, 1, 2, \dots$ λ : expected value

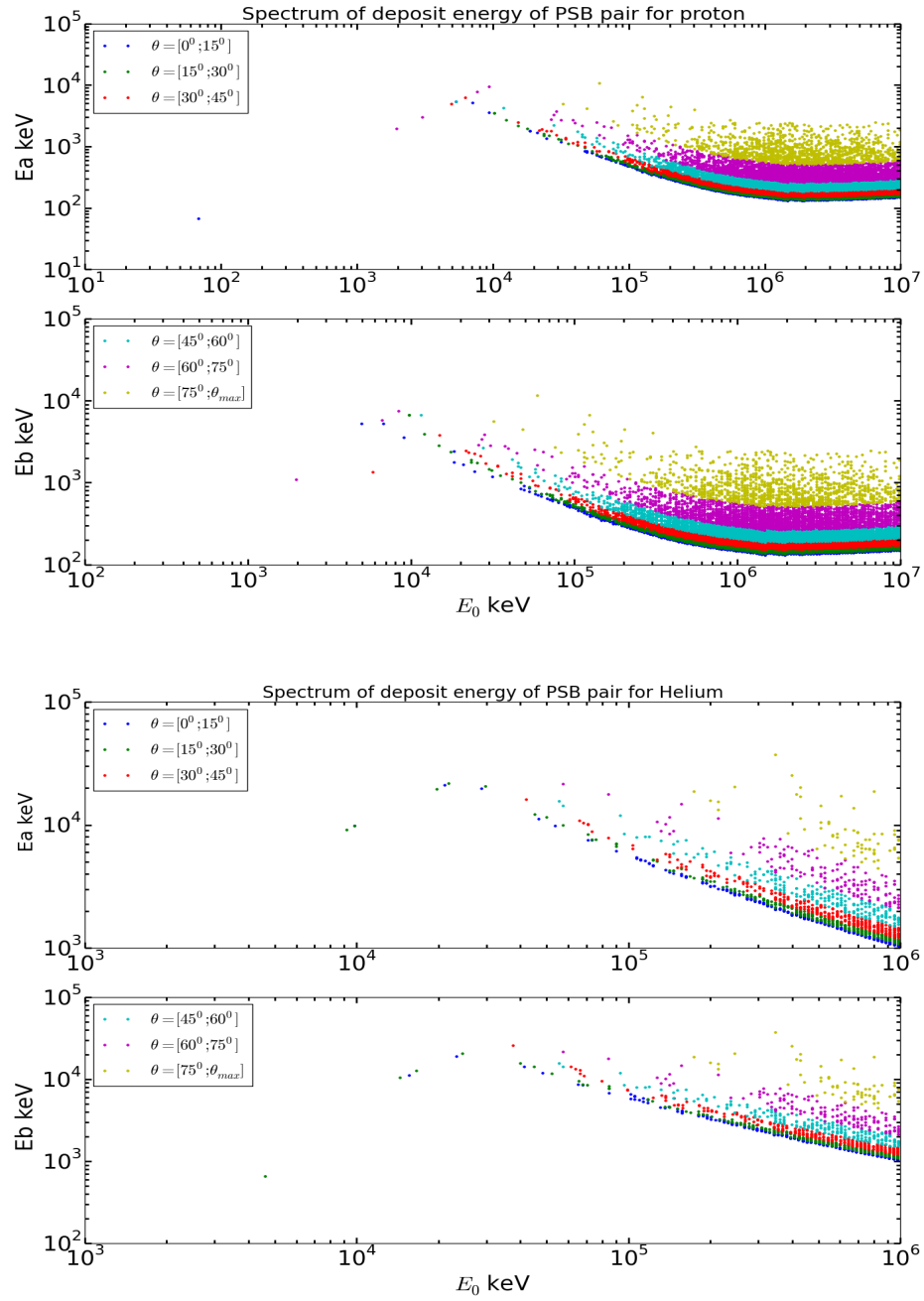


FIGURE 4.8: Deposit energy of p and He between PSB-a and PSB-b

Figure 4.9 shows the simulation method diagram. The cumulative distribution $N(> E)$ of long glitches is also computed using equation 4.2 from numerical calculation. The shape of the long glitches will be shown in chapter V.

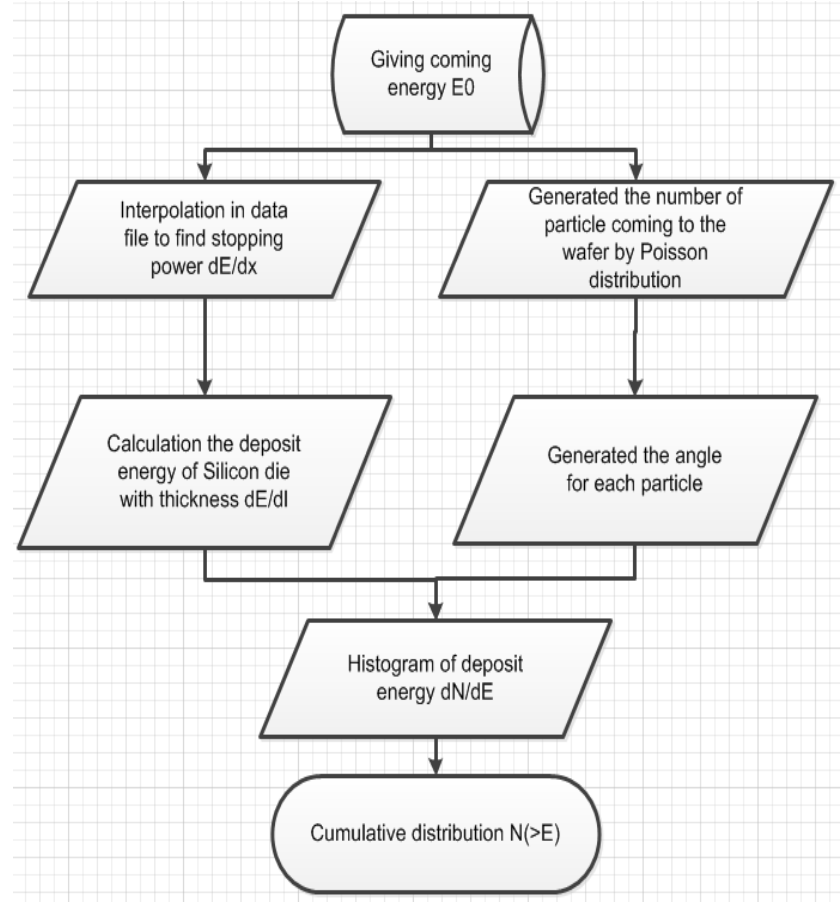


FIGURE 4.9: The flow chart of simulation approach for numerical method

4.4 Coincidences analysis

The simulation approach is used to compute joint interaction between PSB-a and PSB-b. When the protons as well as He interact with the first silicon die with energy E_0 and angle θ , the process is described in the section 3.2.1, it interacts also eventually with the second wafer. If the energy of coming particles is low energy, it will be absorbed by the first wafer. In the other case the energy of coming particles is high enough, it will lose energy at the first silicon die and after that it will be interacted with the second silicon die in the same process. We have measured the deposit energy of each events in PSB-a as well as PSB-b at the same time. We will detect that the event in PSB-a are also detected in coincidence PSB-b. The 2-D histograms of two quantities indicate the coincident event between PSB pair. This work is very important to explain the correlation between PSB a and b observed in data. The result will be shown in chapter V.

Chapter 5

Result, comparison and discussion

The result of theoretical as well as simulation approach will show on this section. Due to the simulation method, we generated the particle coming depend on the time. It mean that when I choose large enough integration time Δt such that statistical errors are small. In principles the simulation approach should converge to the analytical approach when $\Delta t \rightarrow \infty$. On this report I simulate for a week of integration time of Planck satellite.

5.1 Result and comparison

Figure 5.1 indicates the number count for protons and Helium with respect with deposit energy $\frac{dN}{dE}$ in keV unit by analytical (*left*) and simulation (*right*) approach. The energy distribution show power law shape. The range of income energy E_0

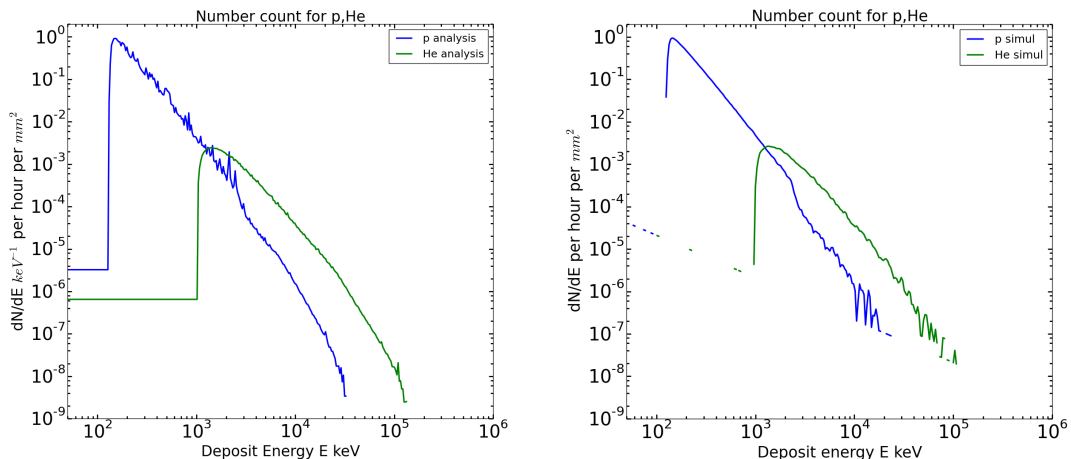


FIGURE 5.1: Spectrum of particle per deposit energy $\frac{dN}{dE}$

for proton is from 10 keV to 10 GeV and from 1 keV to 1 GeV for Helium. The deposit energy minimum around 140 keV and 1.4 MeV for proton and Helium, respectively when the particles coming perpendicular and for which the thickness of the wafer is the smallest. We can see the energy distribution is very steep with power law index -1 between 100 keV and 1 MeV for protons, and -1.7 from MeV to 100 MeV for both proton and Helium.

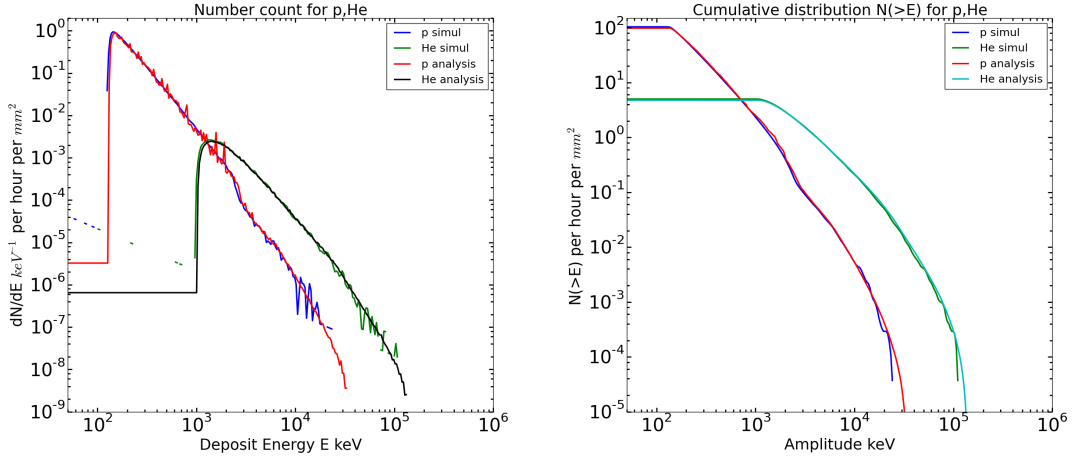


FIGURE 5.2: Spectrum of particle per deposit energy $\frac{dN}{dE}$ and the cumulative distribution $N(> E)$ comparison between 2 approach

We compute $N(> E)$, the number of particles depositing energy $> E$ by integration $\frac{dN}{dE}$. Figure 5.2 indicates that two approaches are fit together. The two methods give the same results. We can see that the proton play a main role at the small deposit energy (>140 keV) and α particle was deposit energy more at the end. It can explain by 4 nucleic number of Helium.

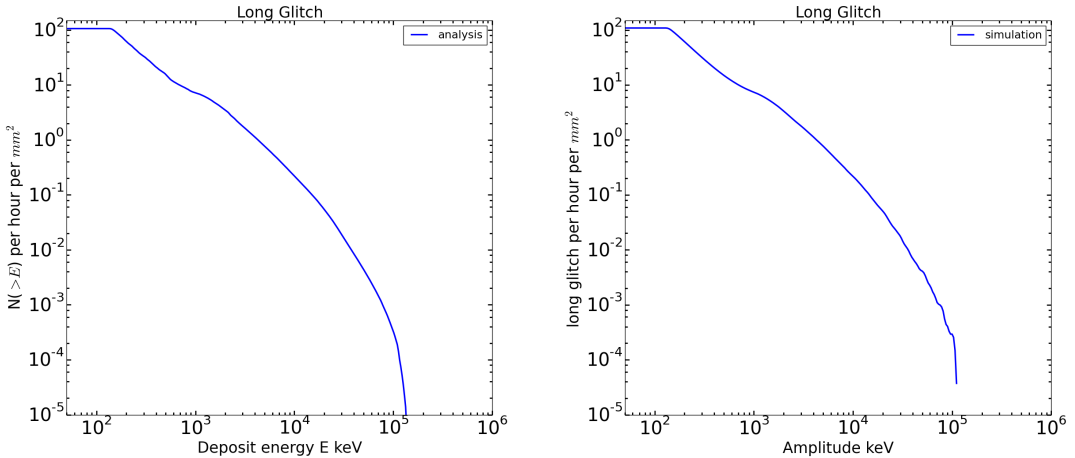


FIGURE 5.3: The long glitches of analytical (left) and simulation (right) for primary CRs.

The geometry of Silicon die is from 40 mm^2 to 80 mm^2 for all bolometer and the integration time $\Delta t - > \infty$. However the long glitch is calculated per an hour per mm^2 therefore the shape is similar for all bolometer. We compare this result with experiment data of the satellite in the figure 5.4. The comparison shows that

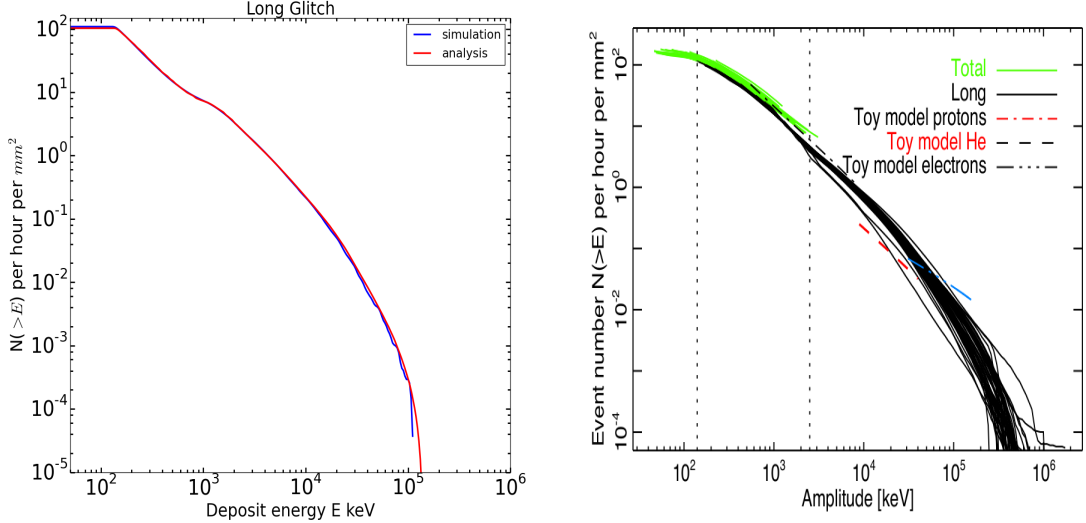


FIGURE 5.4: The long glitches comparison. *left:* Analytical and simulation fit. *right:* The experiment data for several bolometers was public the *Planck* data (Planck Collaboration Result I) [17].

analytical, simulation approach are fitted together. There is different at the tail of the long glitches of model with experiment data and the figure also shows that the maximum value is around 10^2 particles coming per hour per mm^2 on the analytical as well as simulation approach. While it is $1.5 * 10^2$ particles coming per hour per mm^2 on the experiment data. There is something different between analytical, simulation approach and experiment data. I predict it is less high energy particles than seen.

Figure 5.5 shows the evolution of long glitch in integration time $\Delta t = 1 \text{ h}$ for different angle. The plot indicates that the higher angle is higher deposit energy around 10^4 and 10^5 keV. It also indicates that when particles coming perpendicular ($\theta = 0_0$) with the silicon die, the deposit energy is the least and of the number of particles is the highest. However when the angle changes leads to surface effect and length of particles through inside the silicon die change as mention in section 4.1. The result is more energy deposit and the number of particles is smaller than perpendicular direction. The result is discussed in 5.2.

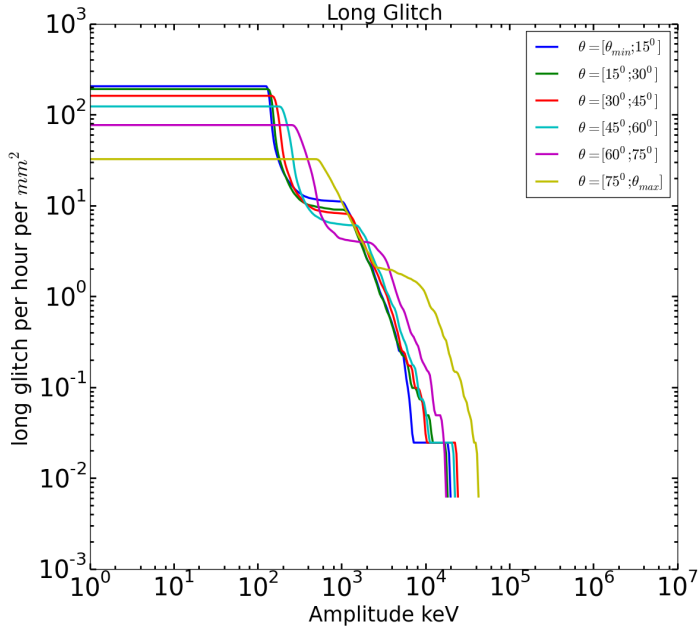


FIGURE 5.5: The long glitches simulate in a PSB pair in integration time $\Delta t = 1$ h for different angle

5.2 Interpretation and Discussion

There is clear evidence that the long glitches result from CRs hitting the silicon die. This is indicated by analytical, simulation and experiment flight ground measurement. The methodology assume the angle sky is 4π for particles come to the silicon die of the satellite but reality the *Planck* bolometer should get less particles than this because of all the material around bolometers. Then the discrepancy between data and model is event large. Meanwhile the maximum number of particles per hour per mm^2 of the methodology is 10^2 compare with $1.5 * 10^2$ of the experiment data (figure 5.4). We could explain that the model is only computed for primary CRs protons and Helium. In the section 3.1 it could indicates that the component of CRs have secondary cosmic rays. Therefore, in fact the maximum number of particles is higher than the assumption leads to the tail of the model is lager than the result in figure 5.4. On the other hand, the secondary particles can be produced by the particles interaction with the matter of the *Planck* satellite. This secondary particles also interact with the wafer and contribute on the observation data.

Another approximation is that the spectrum of particles respect with coming energy $\frac{dN}{dE_0}$ was based on PAMELA result in 2006 while the *Planck* experiment was launched in 2009. The solar activity is lower in the *Planck* mission (figure 4.3) it mean that the intensity of particles is higher. Additional the spectrum of

particles respect with coming energy of PAMELA experiment measured at LEO orbit while the *Planck* satellite placed at L2. Furthermore it cut at $> 39\text{MeV}$ then we have to also refine the input spectrum $\frac{dN}{dE_0}$.

Another limitation is that for a fixed E_0 and θ , we have in reality a spectrum of deposit energy E.

The simple modeling of silicon die in section 4.1 is also not very good assumption. The fact that silicon die has *Absorber* at the center (figure 2.6 and 2.7). It is effect on the temperature change of the bolometer and effect on the signal of the *Planck* satellite.

5.3 Coincident

We computed coincidences events by making the 2 dimension histogram of energy deposition between PSB-a and PSB-b. Figure 5.6 represents the long glitches coincidences in a PSB pair. The x-axis shows the deposit energy events on the PSB a while the y-axis is PSB b and the color bar indicates the number of events energy deposition. This result is achieved for integration time $\Delta t = 7$ days of the *Planck* on the orbit and for primary CRs protons, Helium. We see only some deposit energy events between PSB-a and PSB-b. The color bar indicates that the coincidences deposit energy of proton populate between 100 KeV and 1 MeV. It can reach 10^5 events around 140 keV. On the case of Helium the range is between 1 MeV and 10 MeV around 10^3 events. We compare the coincidences long glitches of

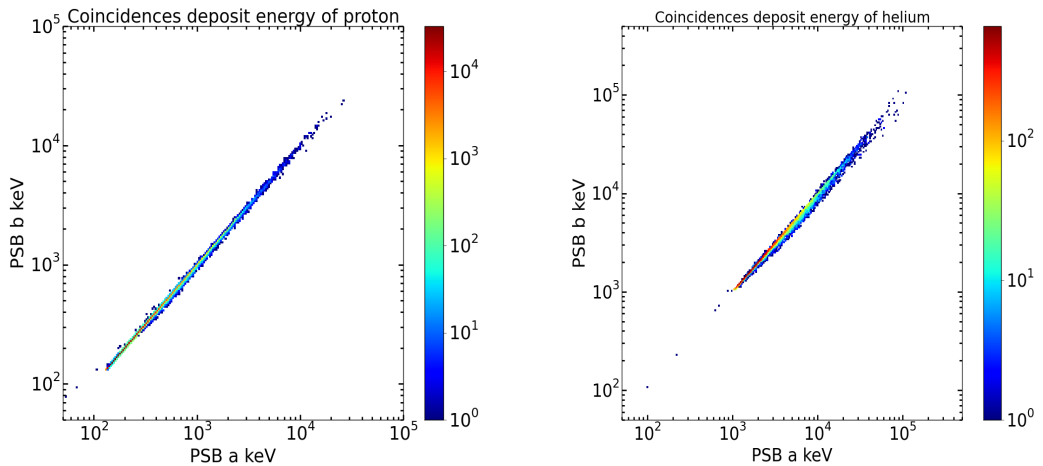


FIGURE 5.6: The long glitches coincident simulate in a PSB pair for proton and Helium

the primary CRs with the experiment data in the figure 5.7. The result shows that

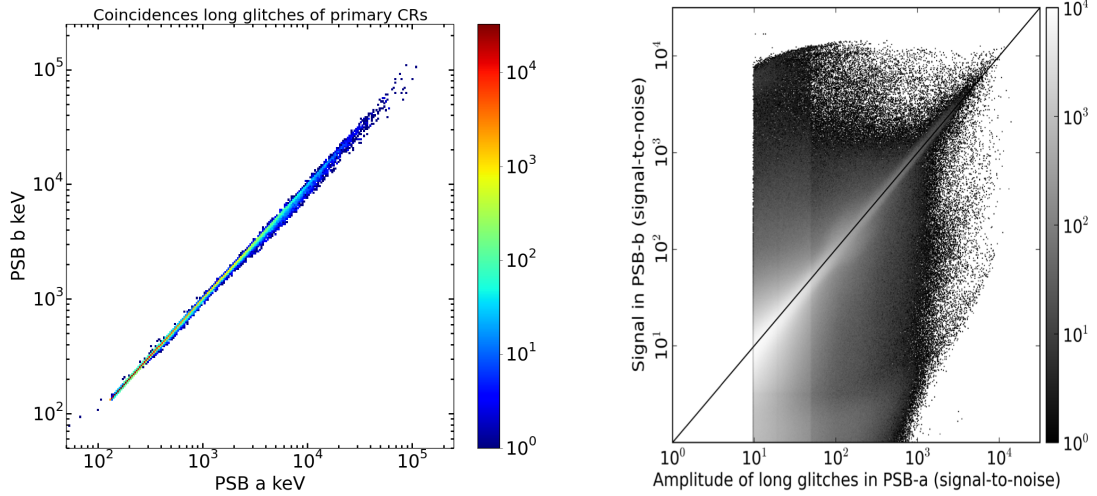


FIGURE 5.7: The long glitches coincident comparison. *left:* Simulation approach *right:* The experiment data in a PSB pair was public the *Planck* data ([Planck Collaboration Result I](#)) [17].

the shape (the diagonal) is similar. The simulation approach only computed for primary CRs protons and Helium while experiment data could have contribution about secondary particles, shower of particles between the first and second wafer and signal to noise. We can predict the different between simulation approach and experiment data in the energy deposition by the fact some low energy events lose a significant fraction, additional the electrons can be ejected from the first silicon die and interact with the second silicon die[17]. I think the result shows that we can not neglect secondary particles.

Chapter 6

Conclusion

In this report, I have developed a simple model of the interaction of galactic particles with the Silicon die of the HFI *Planck* bolometers. I developed a analytical model based of the input spectrum of particles at L2, and modeled the interaction with the silicon die using the stopping power of the material as well as a simulation model to compare with experiment data of the *Planck* satellite.

I predicted the number of events per deposit energy due to primary particles $\frac{dN}{dE}$. I observe good agreements between analytical and simulation method. I predict the correct shape of $\frac{dN}{dE}$ as compare to the data. This is a confirmation that we have a good model of the interaction of CRs with bolometers of Planck satellite and the long glitches result from interaction with the wafer. We can see that the protons are dominated at low deposit energy $> 140\text{keV}$ and the α particles dominated at high energy deposit ($> 1\text{MeV}$). But I do not predict the exact number of particles between model (10^2 total) and observation data ($\approx 1.5 * 10^2$ total) in the data. The difference might be explained by secondary particles interactions and also the model can be improved including more accurate geometry of the wafer (with hold at the center), the solid angle (less than $4 * \pi$). It also could be refine the input spectrum $\frac{dN}{dE_0}$ of the PAMELA result.

I also computed the statistic of the energy of events in coincidence PSB pair as it turn out that the particle penetrate on both PSBa and PSBb are similar. But the model do not predict correct coincidences on data. It could be due to particle shower or population of low energy particles which is not modeled. There could be secondary particles such as electrons which was ejected from the first silicon die and interact with second silicon die.

Finally, the model and observation data may indicates that we can not neglect the secondary particles to explain the discrepancy between the model and the experiment data.

On the other hand, I am thank to the APC laboratory. Here, I have a new computer for working, especially I have opportunity to work beside the PhD students and the professors. Especially my supervisor, associate professor Guillaume Patanchon is always helpful me to improve the knowledge and passion science. This environment impacts on me to learn more and more. Finally the key question 'why it is wrong ?' was improved me during the internship time.

Bibliography

- [1] Planck early results.iv. first assessment of the high frequency instrument in-flight performance. *Astronomy & Astrophysics special feature*, 11.Jan.2011. URL <http://arxiv.org/abs/1101.2039>.
- [2] Record-setting cosmic rays intensities in 2009 and 2010. *The Astrophysics journal letter*, 1.November.2010. URL <http://iopscience.iop.org/2041-8205/723/1/L1/>.
- [3] Energetic particles in the universe; how does nature beat cern? *Plasma physics and controlled fusion*, 20 July 2009. URL <http://iopscience.iop.org/0741-3335/51/12/124005>.
- [4] Pamela measurements of cosmic-ray proton and helium spectra. 21 Mar 2011. URL <http://arxiv.org/abs/1103.4055>.
- [5] Planck 2013 results. xvi. cosmological parameters. *Astronomy & Astrophysics manuscript no. final param paper*, 21 Mar 2014. URL <http://arxiv.org/abs/1303.5076>.
- [6] Planck. vi. high frequency instrument data processing. *Astronomy & Astrophysics manuscript no. HFIDPC*, 26 March 2013. URL <http://arxiv.org/abs/1303.5067>.
- [7] R. Harboe Sorensen A. Mohammadzadeh, B. Nickson. Dedicated instruments to monitor the space radiation environment.
- [8] J. Bock, S. Church, M. Devlin, G. Hinshaw, A. Lange, A. Lee, L. Page, B. Partridge, J. Ruhl, M. Tegmark, P. Timbie, R. Weiss, B. Winstein, and M. Zaldarriaga. Task Force on Cosmic Microwave Background Research. *ArXiv Astrophysics e-prints*, April 2006. URL <http://arxiv.org/abs/astro-ph/0604101>.
- [9] P. Cabella and M. Kamionkowski. Theory of Cosmic Microwave Background Polarization. *ArXiv Astrophysics e-prints*, March 2004. URL <http://adsabs.harvard.edu/abs/2004astro.ph..3392C>.

- [10] A. Catalano, P. Ade, Y. Atik, A. Benoit, E. Bréele, J. J. Bock, P. Camus, M. Chabot, M. Charra, B. P. Crill, N. Coron, A. Coulais, F.-X. Désert, L. Fauvet, Y. Giraud-Héraud, O. Guillaudin, W. Holmes, W. C. Jones, J.-M. Lamarre, J. Macías-Pérez, M. Martinez, A. Miniussi, A. Monfardini, F. Pajot, G. Patanchon, A. Pelissier, M. Piat, J.-L. Puget, C. Renault, C. Rosset, D. Santos, A. Sauvé, L. D. Spencer, and R. Sudiwala. Impact of particles on the Planck HFI detectors: Ground-based measurements and physical interpretation. *ArXiv e-prints*, March 2014. URL <http://arxiv.org/abs/1403.6592>.
- [11] Planck Collaboration. *Planck Explanatory Supplement*. ESA, 2014.
- [12] The Planck consortia. *Planck the Scientific Programme*. ESA, 2005.
- [13] Dr. David Hathaway. Solar cycle prediction. *National Aeronautics and Space Administration*, Updated 2014/06/12. URL <http://solarscience.msfc.nasa.gov/predict.shtml>.
- [14] William R. Leo. *Techniques for nuclear and particle physics experiments*. Springer-Verlag, 1987.
- [15] Andrew Liddle. *An Introduction to Modern Cosmology*. Wiley, 2003.
- [16] A. Miniussi, J.-L. Puget, W. Holmes, G. Patanchon, A. Catalano, Y. Giraud-Héraud, F. Pajot, M. Piat, and L. Vibert. Study of Cosmic Ray Impact on Planck/HFI Low Temperature Detectors. *Journal of Low Temperature Physics*, February 2014. doi: 10.1007/s10909-014-1104-x. URL <http://arxiv.org/abs/1404.1305>.
- [17] Planck Collaboration, P. A. R. Ade, N. Aghanim, C. Armitage-Caplan, M. Arnaud, M. Ashdown, F. Atrio-Barandela, J. Aumont, C. Baccigalupi, A. J. Banday, and et al. Planck 2013 results X. Energetic particle effects: characterization, removal, and simulation. *ArXiv e-prints*, March 2013. URL <http://arxiv.org/abs/1404.1305>.
- [18] Planck Collaboration, P. A. R. Ade, N. Aghanim, C. Armitage-Caplan, M. Arnaud, M. Ashdown, F. Atrio-Barandela, J. Aumont, C. Baccigalupi, A. J. Banday, and et al. Planck 2013 results. XVI. Cosmological parameters. *ArXiv e-prints*, March 2013. URL <http://adsabs.harvard.edu/abs/2013arXiv1303.5076P>.
- [19] James R. Arnold Robert C. Reedy and Devendra Lal. Cosmic-ray record in solar system matter. *Science Journals*, 14 January 1983. URL DOI:10.1126/science.219.4581.127.

- [20] Tauber, J. A., Norgaard-Nielsen, H. U., Ade, P. A. R., Amiri Parian, J., Banos, T., Bersanelli, M., Burigana, C., Chamballu, A., de Chambure, D., Christensen, P. R., Corre, O., Cozzani, A., Crill, B., Crone, G., D’Arcangelo, O., Daddato, R., Doyle, D., Dubruel, D., Forma, G., Hills, R., Huffenberger, K., Jaffe, A. H., Jessen, N., Kletzkine, P., Lamarre, J. M., Leahy, J. P., Longval, Y., de Maagt, P., Maffei, B., Mandolesi, N., Martí-Canales, J., Martín-Polegre, A., Martin, P., Mendes, L., Murphy, J. A., Nielsen, P., Noviello, F., Paquay, M., Peacocke, T., Ponthieu, N., Pontoppidan, K., Ristorcelli, I., Riti, J.-B., Rolo, L., Rosset, C., Sandri, M., Savini, G., Sudiwala, R., Tristram, M., Valenziano, L., van der Vorst, M., van ’t Klooster, K., Villa, F., and Yurchenko, V. Planck pre-launch status: The optical system. *Astronomy & Astrophysics*, 520:A2, 2010. doi: 10.1051/0004-6361/200912911. URL <http://dx.doi.org/10.1051/0004-6361/200912911>.
- [21] X. Dupac and J. Tauber. Scanning strategy for mapping the cosmic microwave background anisotropies with planck. *A&A*, 430(1):363–371, 2005. doi: 10.1051/0004-6361:20041526. URL <http://dx.doi.org/10.1051/0004-6361:20041526>.